Powder Technology 481 (2026) 122688

Contents lists available at ScienceDirect

Powder Technology

journal homepage: www.journals.elsevier.com/powder-technology

Computational optimization of spatial drug release to enhance inhaled particle deposition in human upper and central airways

Ruipeng Xu [a,b], Jiaqi Fan [c,d], Xueren Li [c,d,e], J. Ruud van Ommen [a], Yidan Shang [f,g], Saša Kenjereš [a,b,*]

[a] Department of Chemical Engineering, Faculty of Applied Sciences, Delft University of Technology, Van der Maasweg 9, 2629 HZ Delft, The Netherlands
[b] J.M. Burgerscentrum Research School for Fluid Mechanics, Mekelweg 2, 2628 CD Delft, The Netherlands
[c] School of Safety Engineering, China University of Mining and Technology, Xuzhou 221116, China
[d] Jiangsu Engineering Research Center of Dust Control and Occupational Protection, Xuzhou 221008, China
[e] School of Engineering, RMIT Unversity, PO Box 71, Bundoora, VIC 3083, Australia
[f] School of Mechanical and Automotive Engineering, Shanghai University of Engineering Science, 201620, China
[g] Xuhui Central Hospital, Fudan University, Shanghai 200031, China

HIGHLIGHTS

- A computational framework was developed to optimize aerosol particle release strategies for deep-lung drug delivery.
- Subject-specific mouth-to-lung geometries reconstructed from high-resolution CT scans ensured anatomical accuracy.
- Non-invasive concentrated release at the mouth enhanced particle penetration through the laryngeal constriction.
- Invasive strategies such as catheter-based injection improved particle deposition in deeper lung generations.
- Directional control of deposition was achieved, enabling preferential targeting of left or right lung lobes.
- The results provide a foundation for designing site-specific and patient-tailored inhalation therapies for respiratory diseases.

GRAPHICAL ABSTRACT

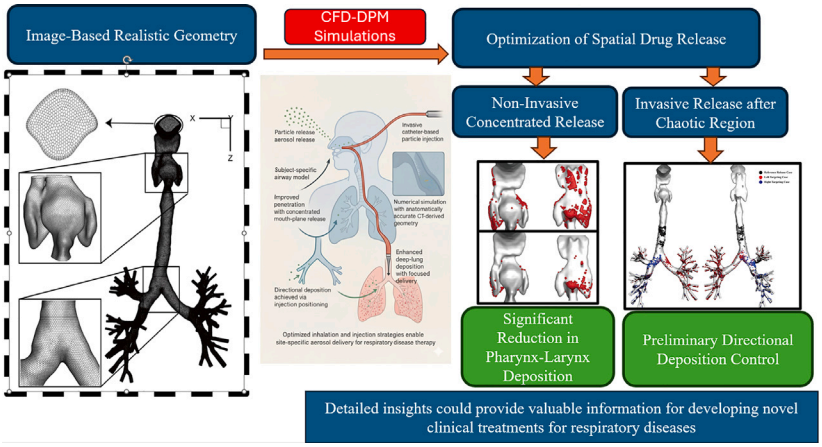

ARTICLE INFO

Keywords:
Lungs
Oral medical drug delivery
CFD
Discrete phase model
Particle deposition

ABSTRACT

Inhaled drug delivery is a promising strategy for the rapid treatment of respiratory diseases due to its direct targeting of the pulmonary system. Nevertheless, challenges remain in optimizing deposition efficiency, particularly in reaching deeper lung generations and achieving directional control of particle transport. To achieve effective deep-lung aerosol delivery, the present proof-of-concept study proposes computational optimization of particle release strategies. Both non-invasive and invasive approaches are explored, with particular emphasis on release concentration and spatial positioning. Numerical simulations are conducted using a previously validated subject-specific mouth-to-lung model reconstructed from high-resolution Computed Tomography (CT) scans, ensuring anatomical realism and geometrical reproducibility. The results show that concentrated non-invasive

* Corresponding author at: Department of Chemical Engineering, Faculty of Applied Sciences, Delft University of Technology, Van der Maasweg 9, 2629 HZ Delft, The Netherlands.
E-mail addresses: r.xu@tudelft.nl (R. Xu), s.kenjeres@tudelft.nl (S. Kenjereš).

https://doi.org/10.1016/j.powtec.2026.122688
Received 21 October 2025; Received in revised form 23 March 2026; Accepted 14 May 2026
Available online 20 May 2026

release at the mouth plane improves particle penetration through the constricted laryngeal region. Meanwhile, invasive strategies involving focused delivery (such as catheter-based injection) lead to enhanced deposition in the deeper lung regions. Notably, directional control of deposition was preliminarily achieved, with particles preferentially targeting either the left or right lung lobe based on the injection position, offering new potential for site-specific therapy. It is concluded that the presented computational framework can provide detailed insights for optimizing particle transport and deposition in specific lung regions. These detailed insights could provide valuable information for developing novel clinical treatments for respiratory diseases.

1. Introduction

The current rapid pace of urbanization has led to a substantial rise in air pollution levels, transforming respiratory diseases into a significant global public health concern. According to a report by the World Health Organization (WHO) [1], over 7 million premature deaths annually are linked to exposure to polluted air, underscoring the severity of the problem. The human respiratory system, as the only internal organ continuously exposed to the external environment, is particularly vulnerable to airborne pollutants. These pollutants enter the respiratory tract through inhalation, triggering a range of health issues from asthma to chronic obstructive pulmonary disease (COPD). Moreover, the structure of the respiratory system makes it susceptible not only to chronic exposure but also to acute infections caused by airborne pathogens.

In addition to chronic pollution-related conditions, the respiratory system is frequently the primary target of emerging infectious diseases. Over the past two decades, the world has experienced three major outbreaks of corona viruses: SARS in 2003, MERS in 2012, and COVID-19 in 2019, each occurring roughly 8 to 10 years apart, highlighting the recurrent threat posed by respiratory viruses. The COVID-19 pandemic, in particular, has heightened global awareness and scientific interest in respiratory health and disease management. Consequently, there has been an exponential increase in research focusing on mechanisms of pollutant transport [2,3], inhalation exposure in occupational and pandemic contexts [4–7], and airflow dynamics related to ventilation performance [8,9].

Among various intervention strategies, inhalation therapy has emerged as a promising modality for managing respiratory diseases. Inhalers are gaining attention due to their ability to deliver medications directly into the lungs, enabling rapid onset of therapeutic action and reducing systemic side effects. Compared to oral or intravenous routes, inhalation allows drug particles to bypass hepatic first-pass metabolism and reach the affected lung tissues more efficiently. However, several challenges persist, including variability in patient inhalation techniques, the complexity of the human airway anatomy, and the difficulty of achieving targeted deposition in the lower airways or specific lung lobes [10].

A critical barrier in inhalation therapy is controlling aerosol particle deposition within the human respiratory tract. Particle fate is governed by multiple parameters, including particle size, shape, release velocity, inhalation pattern, and airway geometry. While larger particles tend to deposit in the upper airway due to inertial impaction, smaller particles can reach the deep lung regions but are prone to exhalation without deposition. Therefore, to optimize therapeutic efficacy and reduce wastage, it is essential to precisely control the location and extent of particle deposition.

To this end, two major research objectives have been previously proposed: (1) a comprehensive analysis of airflow dynamics and particle deposition patterns in the human airway, and (2) the development of active strategies to control and optimize deposition locations [11].

Understanding airflow dynamics and particle deposition in the human airway is essential for advancing respiratory health, optimizing inhaled drug delivery, and evaluating the risks posed by environmental pollutants. Recent progress in computational fluid dynamics (CFD) and experimental methods has provided new insights into these complex processes Researchers have employed various methodologies in the development of medical devices to evaluate the impact of different approaches on particle deposition in the upper respiratory track. However, the scope of these studies has largely been confined to the oropharyngeal region [12]. Airflow in the human airway is strongly affected by anatomical geometry, breathing patterns, and flow rates, producing diverse flow characteristics across regions.

High-velocity zones, particularly in the larynx and at airway bifurcations, generate turbulence and vortical structures that significantly alter particle trajectories and deposition [13–15]. Airflow patterns also differ between transient and steady conditions, with transient effects most pronounced during the deceleration phase of inspiration. Nevertheless, overall deposition fractions for cyclic and steady flows often remain similar at matched flow rates [16–18]. Variability in airflow is additionally observed across successive airway generations, where geometric asymmetries and branching patterns can amplify disturbances and produce cumulative effects over multiple bifurcations [19,20].

The mechanisms governing particle deposition are highly multifaceted, with different physical processes dominating under distinct conditions. Inertial impaction is the primary deposition mechanism for particles larger than 1 μm, especially in the upper airways and at higher flow rates [13,14,21,22], whereas gravitational sedimentation plays a major role for intermediate-sized particles in the lower airways, with efficiency increasing log-linearly with particle size [21]. By contrast, Brownian diffusion dominates for nanoparticles smaller than 0.1 μm, resulting in more uniform deposition patterns and enabling penetration into deeper lung regions [16,22,23].

Deposition has also been correlated with wall shear stress divergence (WSSdiv), which has been shown to predict localized particle retention for physiologically relevant Stokes numbers [24]. In addition to these mechanisms, deposition outcomes are influenced by particle size and morphology [21,23,25], inhalation rate [13,14,22], and pathological airway alterations such as asthma or stenosis. Such conditions increase deposition due to enhanced secondary flows and elevated airway resistance [19,22,26]. Moreover, swirling and helical flows have been reported to either enhance or suppress deposition efficiency depending on injection conditions, with controlled helical flows showing potential to decrease deposition in the oral cavity while improving targeted drug delivery [27,28].

Recent research has introduced several active strategies including novel approaches such as particle shape, size, and surface tuning [29–31] or using of smart inhalers [32] to control and optimize inhaled particle deposition in the human airways, aiming to enhance drug delivery efficacy while minimizing side effects. One promising approach is magnetic targeting, in which therapeutic aerosols are coupled with magnetic particles and guided by external magnetic fields [33,34]. Both in vitro and computational studies demonstrate that this technique can substantially increase targeted deposition, particularly when combined with pulsed aerosol delivery and breath-hold maneuvers [35,36]. The efficiency depends on factors such as magnetic field strength, particle size, and source configuration, with optimized setups significantly enhancing deposition efficiency, as shown in [33,36].

Flow engineering and inhaler design provide another avenue. Introducing controlled helical or swirling flows has been shown to reduce unwanted deposition in the oral cavity. For example, increasing the swirl number decreases deposition of 2 μm particles by up to 73.5% at higher inhalation rates [27,28]. Similarly, spray parameters in pressurized metered-dose inhalers (pMDIs), particularly cone angle, exert a

strong influence on deposition patterns, [37]. Researchers also analyzed the effects of relative velocity between particles and the carrier flow, as well as the shape of inhalers, on de-agglomeration and aerosolization, thereby providing new reference points for optimizing drug delivery efficiency [38].

Personalized inhalation strategies have also been proposed, in which tailored flow profiles or breath-hold maneuvers optimize deposition across particle sizes, [39,40]. Finally, electrostatic charge manipulation has emerged as a complementary method, enhancing deposition in specific airway regions, particularly for submicron particles [41].

Due to ethical constraints and the complexity of *in vivo* experimentation, numerical simulations using Computational Fluid Dynamics (CFD) have become the principal method for investigating these phenomena [42] due to the convenient, low-cost and non-invasive characteristics. Past studies have provided critical insights into geometric modeling and simplification [42], as well as mathematical and turbulence model selection [43–45] and particle tracking methodologies. Two primary numerical approaches have been widely employed to model particle transport. The first is the Euler–Euler method, which treats the particle phase as a continuous medium and tracks changes in mass fraction. This approach is commonly used in pollutant dispersion studies [46]. The second is the Eulerian–Lagrangian approach, which tracks individual particles based on Newton's second law and is well suited for detailed analysis of deposition patterns in the respiratory tract [34,47].

In recent years, machine learning (ML) models have been introduced to estimate particle deposition based on limited CFD data, with regression models demonstrating promising results in providing fast and accurate predictions [48]. While simulation and ML-based prediction offer valuable tools for estimating deposition efficiency, achieving precise control over deposition location, particularly in the lower airway generations beyond generation 8 (G8), remains an open challenge. Previous studies have extensively focused on refining the physical characteristics of particles, such as size, shape, and material properties, to improve deposition efficiency [49–51]. However, relatively few studies have explored optimization strategies based on release parameters, such as concentration distribution and spatial release location.

Some previous studies have also started to focus on particle release strategies, [52]. Efforts in this area include pairing particle release with inhalation rate, [53], and employing invasive equipment to bypass chaotic flow near the human throat, which has also been proposed as a novel approach to optimize particle deposition within the airways, [54]. With the recent advancement of high-resolution lungs imaging techniques, patient-specific treatments for respiratory diseases are also becoming feasible, [55].

Building on these foundations and addressing existing gaps in the literature, the present study evaluates novel strategies for optimizing particle deposition by manipulating initial release conditions. Specifically, it investigates how variations in the spatial distribution and concentration of particles at the release interface influences deposition patterns, with emphasis on targeting regions beyond the 8th airway generation and achieving lateral control toward either the left or right lung. Both non-invasive (oral) and invasive (bronchoscope-assisted) release strategies are considered. The oral route reflects typical clinical and therapeutic practice, whereas the invasive approach is introduced to overcome challenges associated with complex airflow in the laryngeal region and to enhance directional deposition precision.

In summary, the present study integrates CFD modeling, Euler–Lagrangian particle tracing, and particle release strategy optimization to advance the understanding and control of aerosol drug delivery in human airways. This approach aims to provide a robust framework for developing next-generation inhalation therapies capable of achieving personalized and spatially targeted treatment of respiratory diseases.

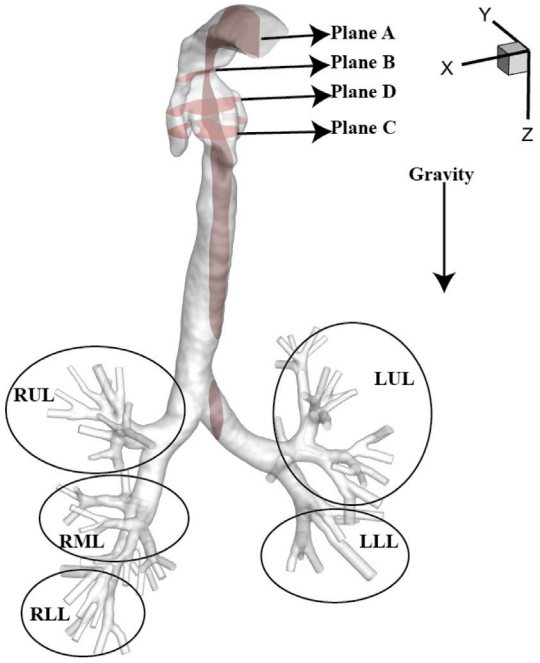

Fig. 1. The realistic lung model considered consists of the upper and central airways (up to the 8th generation), based on the experimental studies of [56]. Planes A–C indicate characteristic locations used for detailed analysis of the obtained results. Similarly, the selected right lung (RL) and left lung (LL) segments, along with their upper, middle, and lower lobes, are also indicated.

2. Method

2.1. Reconstruction of human mouth-lung model

The current study builds upon previous investigations of particle tracking and deposition estimation in the human respiratory system. Specifically, it extends the simulation framework and analysis methodology developed by [33,34], and [57] which are based on experimental work by [56]. The anatomical airway model from [56] serves as the foundational geometry for this research, Fig. 1. The model geometry is based on the CT scans of a healthy 47-year-old male volunteer (174 cm in height and 78 kg in weight).

The model contains several critical anatomical regions, including the extrathoracic airway (oral cavity and pharynx), the upper airway (larynx), and the lower airway, which consists of the trachea bifurcating into the right and left lobes. This model further extends into the lung network, reaching the eighth generation (G8) of bronchial branching. To enable region-specific analysis of particle deposition, the airway model is carefully segmented into anatomically relevant zones, as shown in Fig. 1. Each region is analyzed individually to assess deposition efficiency under different inhalation conditions.

By adopting this validated and anatomically consistent airway model, the present study ensures comparability with previous results while providing a robust framework to extend predictive modeling capabilities, particularly for quantifying regional drug deposition under varying particle injection strategies and parameters. In contrast to similar studies in the literature, the main goal of the present work is to perform a computational optimization of various spatial medical drug release strategies (both invasive and non-invasive) to enhance the deposition of inhaled particles at specific locations within the human lung.

2.2. Simulation methodology

2.2.1. Non-dimensional numbers

The non-dimensional number that characterizes airflow regimes in the airways is the Reynolds number, defined as:

$$Re = \frac{V_0 \cdot D_0}{\nu} \tag{1}$$

where D_0 is the characteristic length scale (in this case, the airway diameter), V_0 is the characteristic velocity and ν is the kinematic viscosity. To describe particle behavior, two non-dimensional parameters are commonly introduced: the Stokes number and deposition efficiency. The Stokes number represents the ratio of particle to fluid relaxation times and signifies the particles ability to follow fluid streamlines:

$$St = \frac{\tau_p}{\tau_f} = \frac{\tau_p U_m}{R} = \frac{C_c \rho_p d_p^2 U_m}{18 \mu_f R} \tag{2}$$

where C_c is the Cunningham slip correction factor. This factor is typically taken as $C_c = 1$ for particles with $d_p > 1$ μm, as applied in [58]. For the single sub-micrometer case considered in this study ($d_p = 0.5$ μm), a value of C_c =1.16 was used for the Stokes number calculation.

The second parameter, deposition efficiency, is defined as:

$$\eta_{\text{dep}} = \frac{\text{particles deposited}}{\text{particles released}} \tag{3}$$

2.2.2. Turbulent airflow model

In this study, steady-state airflow simulations with a flow rate of 60 L/min are first performed in accordance to previous literature [56]. The representing inlet Reynolds number in current simulation reaches the value of Re = 4350 indicating a developed turbulent regime. To capture turbulence effects, we applied the two-equation RANS $k-\omega$ shear-stress transport (SST) closure with enhanced wall treatment. The complete set of governing equations is given next, [59,60].

Mass conservation:

$$\frac{\partial U_i}{\partial x_i} = 0 \tag{4}$$

Momentum equation:

$$\frac{\partial \left(\rho U_i\right)}{\partial t} + \frac{\partial \left(\rho U_i U_j\right)}{\partial x_j} = -\frac{\partial p}{\partial x_i} + \frac{\partial}{\partial x_j}\left[\mu\left(\frac{\partial U_i}{\partial x_j} + \frac{\partial U_j}{\partial x_i}\right) - \rho\overline{u_i' u_j'}\right] \tag{5}$$

Turbulent kinetic energy:

$$\frac{\partial(\rho k)}{\partial t} + \frac{\partial \left(\rho k U_j\right)}{\partial x_j} = \frac{\partial}{\partial x_j}\left[\Gamma_k \frac{\partial k}{\partial x_j}\right] + G_k - Y_k + S_k \tag{6}$$

Specific dissipation rate:

$$\frac{\partial(\rho\omega)}{\partial t} + \frac{\partial \left(\rho\omega U_j\right)}{\partial x_j} = \frac{\partial}{\partial x_j}\left[\Gamma_\omega \frac{\partial \omega}{\partial x_j}\right] + G_\omega - Y_\omega + S_\omega \tag{7}$$

Here, G_k and G_ω represent the generation of the turbulence kinetic energy and of the specific dissipation rate, respectively. S_k and G_ω are user-defined source terms, while Y_k and Y_ω are the dissipation of k and ω resulting from turbulence. Finally, Γ_k and Γ_ω are the effective diffusivity. Standard values of the model coefficients are used and complete overview of the turbulence model is given in [59,60]. This turbulence model has been applied in the previous research resulting in acceptable balance between computational cost and accuracy compared to the high-fidelity large eddy simulation turbulence simulation (LES) techniques, [33,34].

2.2.3. Particle tracking

In current research, the study on the transport and the deposition of inertial particles plays a crucial role. Based on the requirement that one needs to track a particle from a starting release point to the final destination deep in the lungs, we selected the Eulerian–Lagrangian approach. The details of the Eulerian approach for the fluid phase are already addressed in the previous section, and here we focus on the details of applied Lagrangian approach. Here, we will use the one-way coupled approach, i.e. particles will not influence the airflow, which is justifiable due to small volume fraction of the particulate phase. The spherical particle trajectories are reconstructed by solving the equation of motion for each particle, which is based on the second Newton's law, and can be written as:

$$m_p \frac{d\vec{u}_p}{dt} = \sum \vec{F}_i \tag{8}$$

The $\sum \vec{F}_i$ term includes all forces acting on the particle. In the current study we include contributions of the drag ($\vec{F}_D$), gravitational ($\vec{F}_g$), and pressure gradient ($\vec{F}_{\nabla P}$) forces, which are calculated as follows:

$$\vec{F}_D = \frac{m_p f}{\tau_p}\left(\vec{u}_f - \vec{u}_p\right) \tag{9}$$

$$\vec{F}_g = m_p \vec{g} \tag{10}$$

$$\vec{F}_{\nabla P} = m_p \left(\frac{\rho_f}{\rho_p}\right) \frac{D\vec{u}_f}{Dt} \tag{11}$$

where f is the drag factor defined as:

$$f = \begin{cases} 1 & , Re_p \le 1 \\ Re_p^{0.354} & , 1 < Re_p \le 400 \\ 1 + 0.15 Re_p^{0.687} + \frac{0.0175}{1+4.25\cdot 10^4 Re_p^{-1.16}} & , 400 < Re_p \le 3\cdot 10^5 \end{cases} \tag{12}$$

and Re_p is the particle Reynolds number, defined as:

$$Re_p = \frac{\rho_f d_p}{\mu_f}\left|\vec{u}_f - \vec{u}_p\right| \tag{13}$$

In the present work, we assume that particles are spherical and that rotation and collision between particles is negligible. Additional important mechanism that affects the particle movement is the turbulent dispersion. Here, we adopt the discrete random walk (DRW) model, which describes the interactions between particles and turbulent eddies. The turbulent eddies are characterized with a Gaussian distribution of random velocity fluctuations (u', v', w') and characteristic turbulent eddy time scale (τ_e). For the two-equation $k-\omega$ SST model, turbulent dispersion term is calculated as:

$$u' = \zeta\sqrt{\overline{u'^2}}, \quad v' = \zeta\sqrt{\overline{v'^2}}, \quad w' = \zeta\sqrt{\overline{w'^2}} \tag{14}$$

where ζ is a normally distributed random number, and where isotropic distribution of velocity fluctuations is assumed:

$$\sqrt{\overline{u'^2}} = \sqrt{\overline{v'^2}} = \sqrt{\overline{w'^2}} = \sqrt{\frac{2}{3}k} \tag{15}$$

The characteristic lifetime of the turbulent eddy is calculated as:

$$\tau_e = 2T_L, T_L = C_L \frac{k}{\varepsilon} \tag{16}$$

with $C_L = 0.15$, and $\varepsilon = 0.09\omega k$, as reported in [59].

2.3. Mesh generation and boundary conditions

In this study, the reconstructed patient-specific airway model was discretized using the commercial multi-physics analysis software ANSYS Fluent 2022 R2, utilizing its built-in meshing capabilities as shown in Fig. 2. To achieve high-fidelity spatial resolution while maintaining computational feasibility, a polyhedral mesh structure was adopted

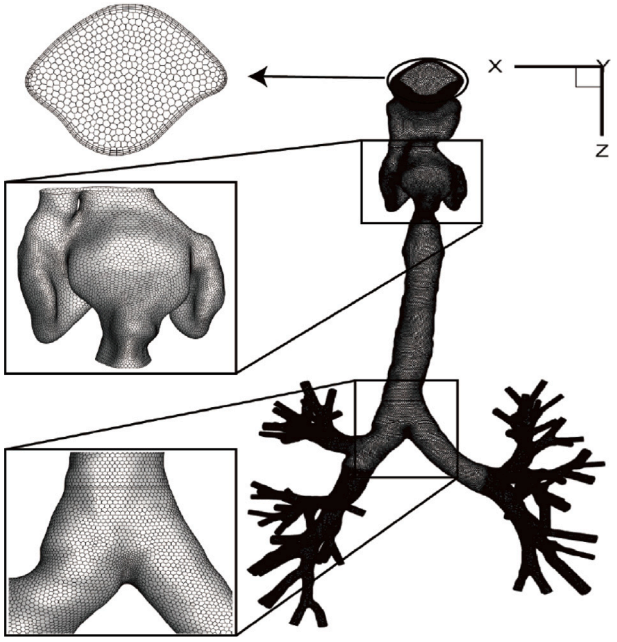

Fig. 2. Mesh preview of the patient-specific lung geometry.

throughout the computational domain. The characteristic control volume cell size for most mesh elements ranged from 0.05 mm to 0.1 mm, ensuring sufficient refinement in both the upper and lower airway branches. Compared to traditional tetrahedral meshes, polyhedral meshes offer enhanced numerical stability and reduced sensitivity to skewness and cell distortion. These advantages make them particularly well-suited for resolving airflow within anatomically complex, multi-scale respiratory geometries, such as sharp curvatures in the pharynx or narrow passages near the larynx and bronchial bifurcations, as demonstrated in [61].

In addition to the core polyhedral elements, five prism layers with an aspect ratio of 5 were implemented adjacent to all wall surfaces to more effectively capture near-wall gradients. These layers are essential for accurately resolving variables such as wall shear stress, pressure drop, and local particle deposition, all of which are highly sensitive to boundary layer development.

To ensure the robustness and numerical accuracy of the simulation results, a comprehensive mesh independence study was carried out using three different mesh densities: Coarse Mesh (0.86 million control volumes), Medium Mesh (1.46 million control volumes), and Fine Mesh (3.1 million control volumes).

As illustrated in Fig. 3, the medium and fine meshes demonstrate a high level of agreement across both the vertical and horizontal velocity profiles at a selected plane in the pharynx–larynx region. This specific location was chosen as it represents the most complex flow field within the simulation domain. Considering the balance between numerical accuracy and computational efficiency, the medium mesh, consisting of approximately 1.46 million polyhedral elements, was selected for the subsequent CFD and particle-tracking simulations.

The scenario simulated in the current research includes a steady breath-in condition (to mimic experimental conditions presented in [56]) combined with the aerosol injection. The detailed boundary condition and particle properties are summarized in Table 1.

Fig. 4 illustrates the spatial configurations and particle distributions for non-invasive release scenarios along the mouth inlet. The left side of the figure presents four representative particle release patterns, labeled as Cases 1 through 4, each demonstrating distinct spread and particle density. These patterns simulate varying dispersion intensities and initial spatial concentrations of particles released at the

Table 1
Summary of boundary conditions and particle properties.

Boundary conditions:	
Inlet	Uniform velocity profile, $Re_{ref} = 4360$, $\phi_v = 60$ L/min, $t_i = 5\%$, $\nu_t/\nu = 10$ [–]
Wall	No-slip condition for fluid
Outlets	Zero gauge pressure
Fluid Properties:	
Density, ρ_f	1.185 kg/m^3
Dynamic viscosity, μ_f	1.82×10^{-5} Pa s
Temperature, T_f	293 K
Particle Properties:	
Density, ρ_p	1000 kg/m^3
Diameter, d_p	(0.5–10) μm single size in each injection

mouth entry. Case1 corresponds to a wide, dense (high-probability) dispersion zone, in which most particles deposit within the targeted human airway region. Conversely, Case4 represents a narrowly focused, low-density (low-probability) distribution. Particles injected in this region more easily penetrate the pharynx–larynx area, as demonstrated by the reverse-tracking profile in Fig. 4. The term 'density' in this context refers to the spatial concentration of deposition probability at the inlet plane, rather than the physical density of the particle material. The injection pattern follows a random-uniform protocol for all subsequent cases (Cases 1–4). Injection locations are generated in a polar coordinate system with a random radial distribution (distance from the center) and a uniform angular distribution, thereby mimicking the stochastic nature of localized drug-spray applications. The right side of the figure shows a cross-sectional view of the oral cavity with superimposed color-coded contours indicating the relative positions of the four cases at the mouth inlet. The reference case, marked in black, serves as the baseline for evaluating the impact of release location on subsequent particle transport and deposition.

The 'backtracking' (or reverse-tracking) analysis was conducted using the individual particle history data recorded. By linking the final deposition coordinates of each particle to its corresponding initial injection coordinates, we were able to isolate and map the specific release locations at the inlet that resulted in deposition within the pharynx–larynx region. This spatial mapping allows us to visualize the 'deposition probability' of the inlet cross-section, as presented in the reference case in Fig. 4.

Colored trajectories indicate the radial offset from the central axis, with Case 1 (red) exhibiting the most peripheral release zone and Case 4 (purple) located near the central region. This configuration study provides a systematic investigation of how varying initial particle distributions affect downstream deposition behavior in the upper and central airways, facilitating optimization of drug delivery strategies via non-invasive oral routes.

3. Results and discussions

3.1. Airflow pattern and particle deposition validation

To ensure reliability of the simulation model, the airflow field and total particle deposition efficiency are validated against previously performed experimental [56] and numerical simulation [34] results. A qualitative comparison of normalized velocity magnitude is shown in Fig. 5. The simulation was carried out with the same experimental mass flow rate of 60 L/min. Three representative cross-sections were selected at the following coordinates: x = −0.255 m (Plane A - vertical plane), z = 0.118 m (Plane B) and z = 0.146 m (Plane C), as indicated in Fig. 1. The selected horizontal planes correspond to locations where the airflow exhibits particularly complex patterns, such as the entrance and exit regions of the larynx. Overall, the present simulation shows very good agreement with experiments at all locations, Fig. 5. Minor local

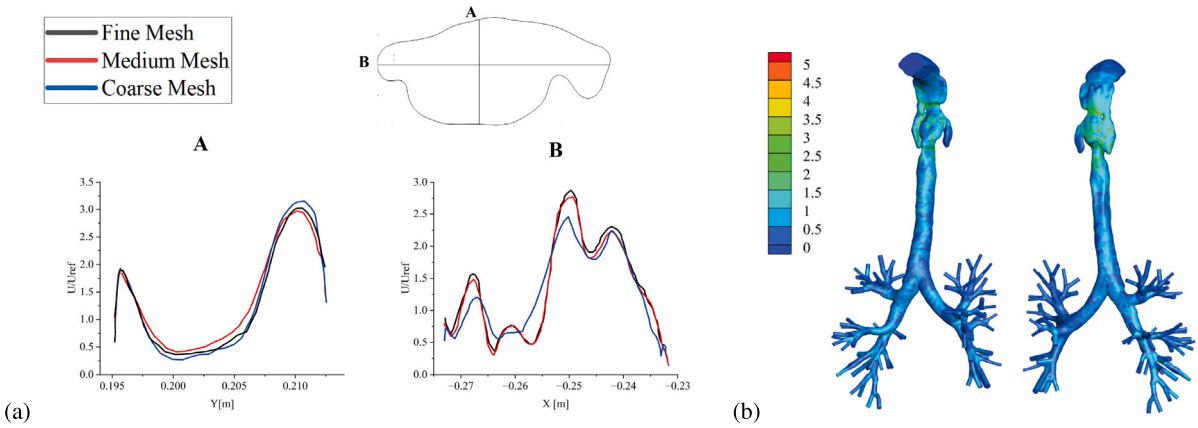

Fig. 3. (a) Mesh independence study of the current simulation model, showing the non-dimensional velocity magnitude ($|U|/U_{ref}$) at Plane D (z = 0.135 m) along vertical (A) and horizontal (B) profiles. (b) Contours of the non-dimensional wall distance (y+) for the fine mesh: front view (-left), back view (-right).

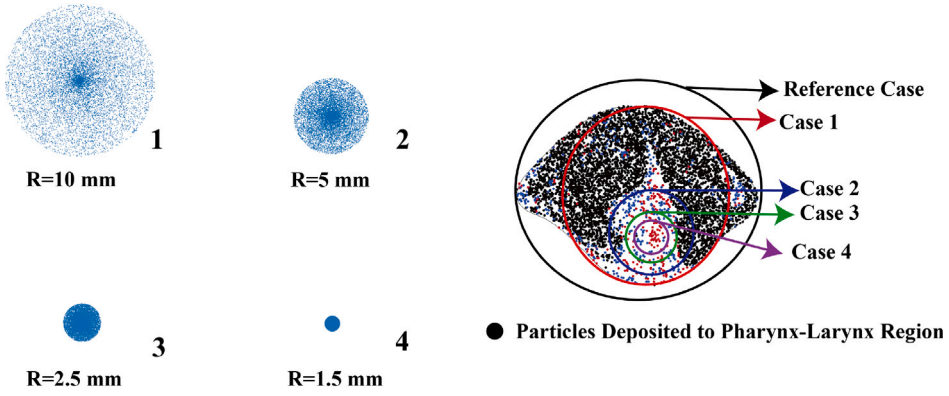

Fig. 4. Particle distribution of non-invasive release and relative locations along the mouth inlet with Random-Uniform Distribution (-left); Backtracking of particles deposited in the pharynx/larynx region (-right). Note that the Case1 through Case4 and their corresponding colors match the distributions shown on the left.

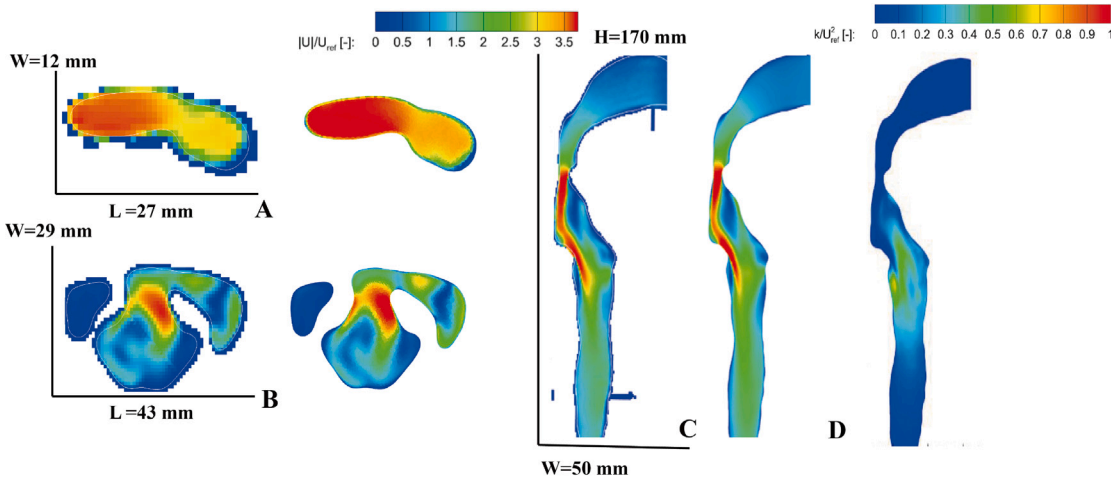

Fig. 5. Contours of the non-dimensional velocity magnitude ($|U|/U_{ref}$) in characteristic horizontal (A,B) and vertical (C) planes are shown alongside the experimental results of [56]. The contours of non-dimensional turbulent kinetic energy (k/U_{ref}^2) in the vertical plane (D) are calculated using the present $k-\omega$ SST model. Note that W, L and H denote the characteristic width, length, and height of the cross-sections, respectively.

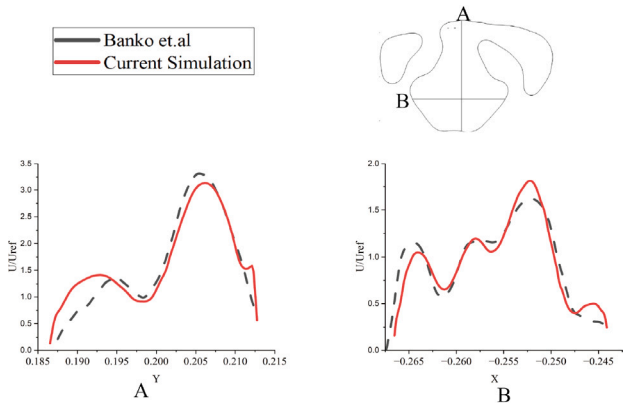

Fig. 6. Comparison of non-dimensional velocity magnitude profiles between the current simulation and experimental data by Banko et al. [56] extracted along the lines A and B in Plane C.

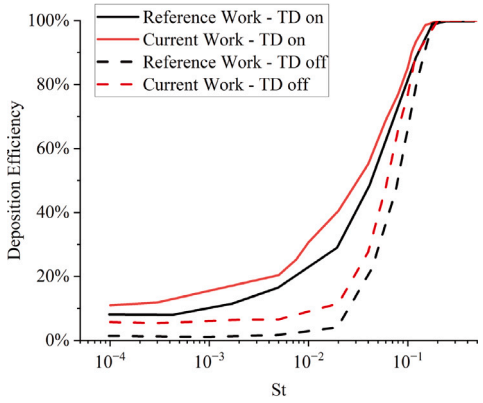

Fig. 7. The total particle deposition efficiency dependence on the Stokes number (St). The impact of the turbulence dispersion (TD) and comparison with numerical results of [34].

discrepancies can be attributed to the use of a relatively simple RANS-type turbulence model. Further quantitative analysis of the velocity field is performed by comparing the velocity magnitude extracted in plane (C) along profiles (A) and (B), as shown in Fig. 6. Again, good agreement is observed with the experimental data for both profiles, with the characteristic peaks properly captured.

With the confirmed good agreement between the simulated airflow patterns and experimental results, we proceed to validate the total particle deposition efficiency. For this validation, we maintained the inlet mass flow rate, characteristic particle diameter (d_P), and density (ρ_p) identical to those used in the literature Ref. [34], ensuring the same Stokes number. Furthermore, the same particle release method (Random-Uniform) and inlet plane were selected, as shown in Fig. 4. Overall, good agreement was obtained with the reference results, Fig. 7. The inclusion of turbulent dispersion (TD) significantly increased the total deposition efficiency for particles within the range $10^{-3} \leq St \leq 5 \times 10^{-2}$. As before, some small deviations can be associated with differences in numerical mesh used, the number of particles released, as well as the underlying airflow turbulence model.

3.2. Analysis of concentrated particles release using a non-invasive approach

Next, we focus on performing a detailed analysis aimed at achieving targeted deposition of particles by manipulating the injection area at the inlet plane, as illustrated in Fig. 4. This approach is based on tracing back the deposited particles from the reference case to the inlet plane. By analyzing the inlet plane, regions with lower particle concentrations (which correspond to non-deposited particles capable of penetrating deeper into the lungs) are identified as promising release areas. Subsequently, we performed a series of simulations with varying release

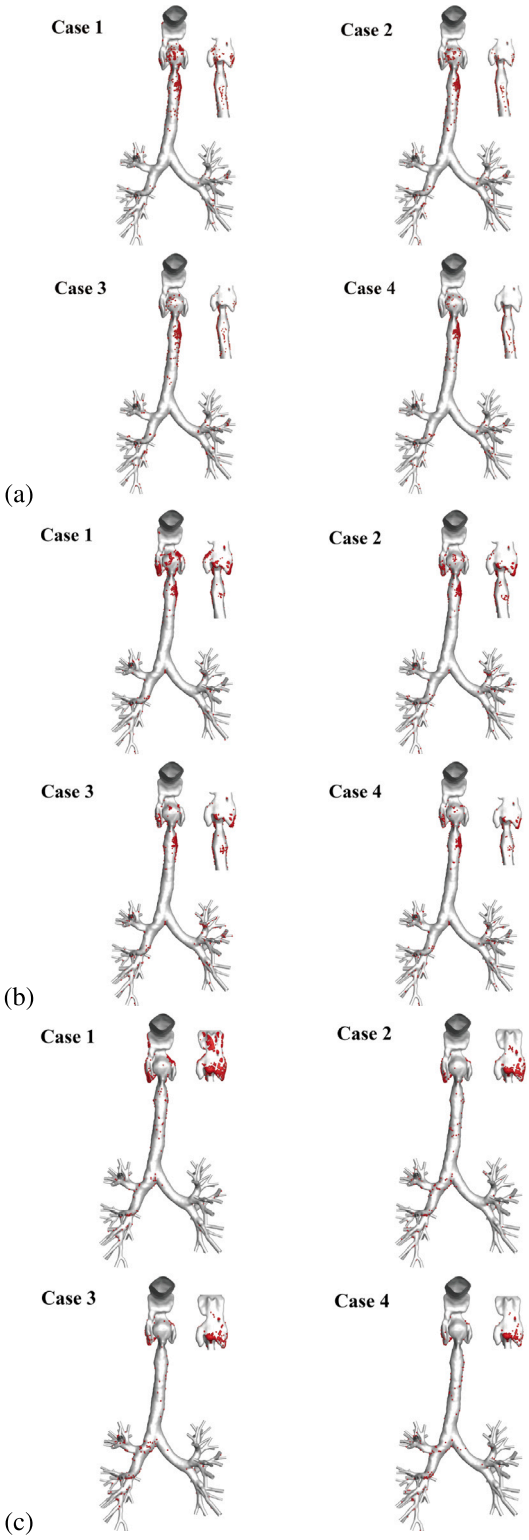

Fig. 8. Local particle deposition for targeted release strategies with different particle sizes: (a) dp = 0.5 μm, (b) dp = 5 μm, (c) dp = 10 μm. The smaller plots show the back view.

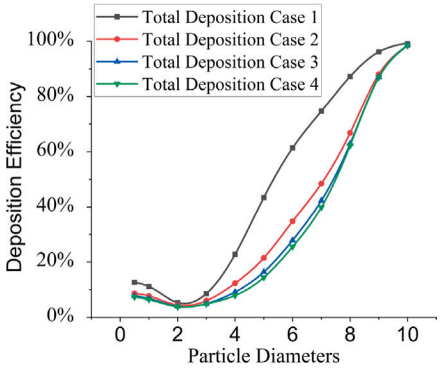

Fig. 9. Total deposition variation for non-invasive concentrated release cases at the inlet plane (mouth region, as shown in Fig. 4). The highest reduction was recorded at $d_P = 5$ μm with a reduction from 43.41% to 14.44%.

radii at the inlet plane (ranging from Case1 to Case4, as illustrated in Fig. 4) and different particle sizes ($0.5 \leq d_p \leq 10$ μm).

Local particle deposition patterns for the selected release strategies (Case1–Case4) and three particle size classes ($d_P = 0.5, 5, 10$ μm) are illustrated in Figs. 8(a) to 8(c). It is observed that particles with diameters $d_P = 0.5$ and 5 μm (Figs. 8(a) and 8(b)) deposit primary within the laryngeal region. In contrast, particles with $d_P = 10$ μm typically deposit before reaching this region, with very few successfully penetrating deeper into the respiratory tract, Fig. 8(c).

This observation is further supported by the analysis of total deposition efficiency across the different release cases and particle diameters, as shown in Fig. 9. Notably, significant differences are obtained between Case1 and the remaining release strategies for $3 \leq d_p \leq 9$ μm, where the deposition efficiency is reduced by up to 50%, indicating that stronger penetrative capabilities are achieved. For smaller particles ($d_P \leq 3$ μm), the differences between the release strategies are minimal, resulting in nearly identical deposition distributions for Case2 through Case4.

Given the complex airflow patterns in the pharynx and larynx regions, the particle distribution is expected to be chaotic and similar across Cases 2 to Case4. This was confirmed by the sectional deposition results shown in Fig. 10. Numerical data show a slight improvement in deposition and escape rates for small and medium-sized particles, likely due to reduced deposition in the pharynx and larynx. Beyond the larynx, the chaotic turbulent flow leads to minimal differences in the section-wise distribution of deposited and escaped particles. For larger particles, most deposit in the larynx or on the tracheal wall before reaching the carina. Therefore, analyzing the escape rates for these particles is not meaningful due to very limited sample size.

Overall, concentrated release demonstrates potential for improving particle penetration through the pharynx and larynx, especially for medium-sized particles. This suggests an opportunity to optimize deposition efficiency in breath-powered drug delivery. However, because of the turbulent, chaotic-like distribution after the larynx, the improvement from the non-invasive concentrated release strategy is still rather limited.

3.3. Invasive release after the larynx region

Although non-invasive treatment is generally preferred in medical treatments, invasive approaches still need to be considered due to the limited performance of non-invasive release demonstrated in the previous section. With recent advancements in medical endoscopic techniques, particularly the use of bronchoscopes, it has become feasible to deliver dry powder aerosols directly into the central airways. Examples include laryngeal injection [62] and the use of endotracheal catheter [54] to release particles deeper within the upper airways.

Further analysis was conducted to achieve significant improvements in particle deposition at deeper airway generations and to enhance directional control. As a proof of concept, the release location was set at a plane corresponding to the local coordinate z = 0.18 m, positioned to avoid flow expansion and the turbulent wake downstream of the larynx, while remaining upstream of the carina in the trachea to enable a controlled and consistent release pattern.

The visualization of particle deposition was first conducted for three classes of particles, following the same classification as in the previous

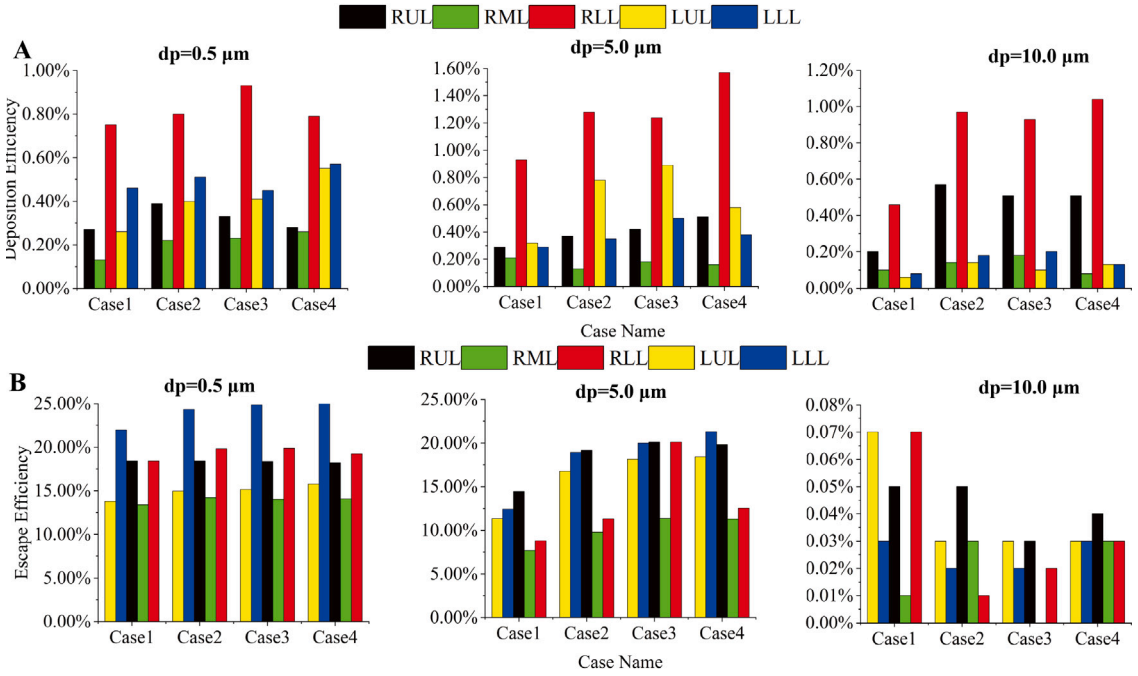

Fig. 10. Sectional deposition and release chart for selected particle diameters and non-invasive delivery. The lung sections are defined according to Fig. 1: RUL — right upper lobe; LUL — left upper lobe; RML — right middle lobe; RLL — right lower lobe; LLL — left lower lobe;.

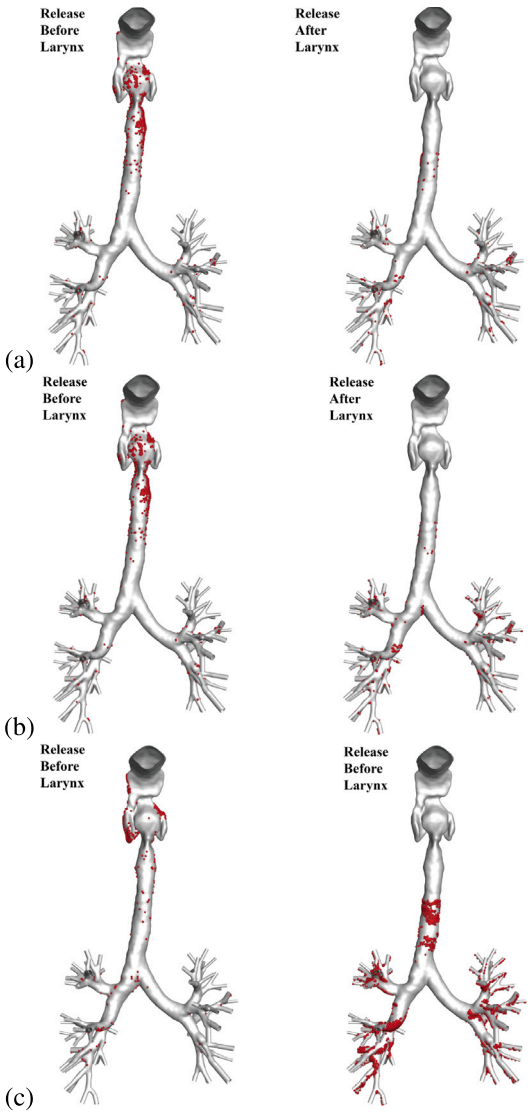

Fig. 11. Comparison of the local particle wall deposition for non-invasive (before larynx) and invasive (after larynx) release for different classes of particles: (a) dp = 0.5 μm, (b) dp = 5 μm, (c) dp = 10 μm.

case. As shown in Fig. 11, particle deposition significantly increases in the sections downstream of the carina across all particle classes. For the large particles (d_P = 10 μm), there is a significant local increase in deposition along the trachea near the release plane, Fig. 11(c). The total deposition efficiency is now compared with the reference case (non-invasive release at the mouth inlet plane, Case1), as shown in Fig. 12. It can be observed that the total deposition efficiency significantly decreases for medium- and large-sized particles, indicating enhanced penetration deeper into the lungs. A reduction of up to 50% is achieved even for particles with d_P = 10 μm. Additionally, an asymptotic deposition efficiency regime is observed for relatively small sized particles, i.e. $0.5 \leq d_p \leq 4$ μm.

Similarly to the non-invasive cases, a detailed analysis was performed for various lung sections, as shown in Fig. 13. For small particles (d_P = 0.5 μm), only marginal changes in total deposition efficiency and escaped particles were observed between the before and after larynx release strategies. In contrast, for large particles (d_P = 10 μm), there was a significant increase in the percentage of escaped particles with the after-larynx release, whereas this number was practically zero for the before-larynx release. For intermediate particle size (d_p = 5 μm), a

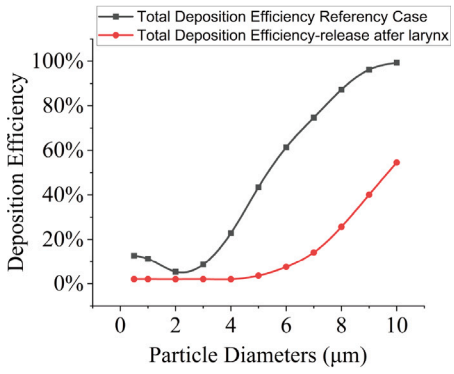

Fig. 12. Total deposition efficiency variation for different particle sizes: comparison between the reference case (inlet at the mouth plane, Case1) and the after-larynx release plane, both including turbulent dispersion effects.

significant increase in escaped particles is also observed for the after-larynx release, Fig. 13, further confirming the feasibility of the invasive approach.

3.4. Directional deposition through invasive release

To achieve reverse tracking of the deposited particles, the process started by identifying potential regions where most particles accumulated on a specific side of the lung. Next, a target release region was selected, and an equivalent amount of particles was released to represent the specified concentration. Reverse tracking was then conducted for each release scenario to assess the effectiveness of directional control (see steps shown in Fig. 14).

The results are presented in Fig. 15. It can be seen that there were significantly different patterns of local deposition depending on the directional strategy, i.e. targeting the left versus the right part of the lung, Fig. 15(a). A detailed overview of the escaped particles, which indicates efficient targeting deeper into the lungs, is shown in Fig. 15(b). When comparing the reference release case (uniform) with the right lung targeting case, an increase was obtained for all right lung lobes, reaching almost a threefold increase in the specifically targeted RUL region. Similarly, for left lung targeting, both the LUL and LML regions showed approximately a twofold increase in escaped particles.

It can be concluded that the proposed invasive after-larynx directional release of particles may serve as powerful and efficient method for controlled delivery of the medical drug to specifically selected regions of the lung.

4. Current limitations

The current simulation employed static inlet conditions to mimic experimental study of [56]. This simplification was justified due to observation that particle residence times within the modeled geometry were shorter than the typical breathing or breath-hold cycles during inhaler use or clinical treatment, resulting in minimal expected impact on particle deposition patterns for tested particle size range. Nevertheless, while this approximation can introduce minor deviations, fully transient flow modeling is recommended for cases requiring high-precision deposition calculations, such as patient-specific lung cancer therapies.

To capture turbulence effects, the RANS-type two-equation $k-\omega$ SST model applied here proved to be a good compromise between accuracy, numerical robustness, and computational efficiency. For a more accurate representation of local turbulence, high-fidelity simulations such as Large Eddy Simulation (LES) or hybrid RANS/LES approaches can be employed.

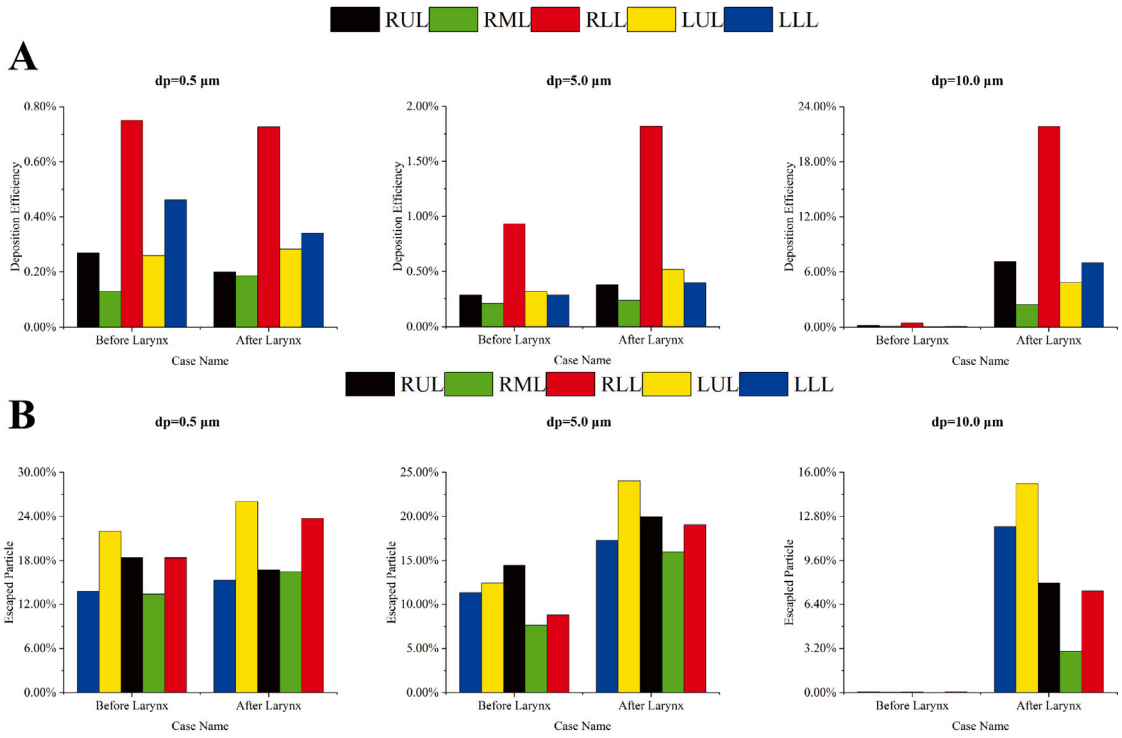

Fig. 13. Sectional deposition and release chart for selected particle diameters and invasive release (after larynx).

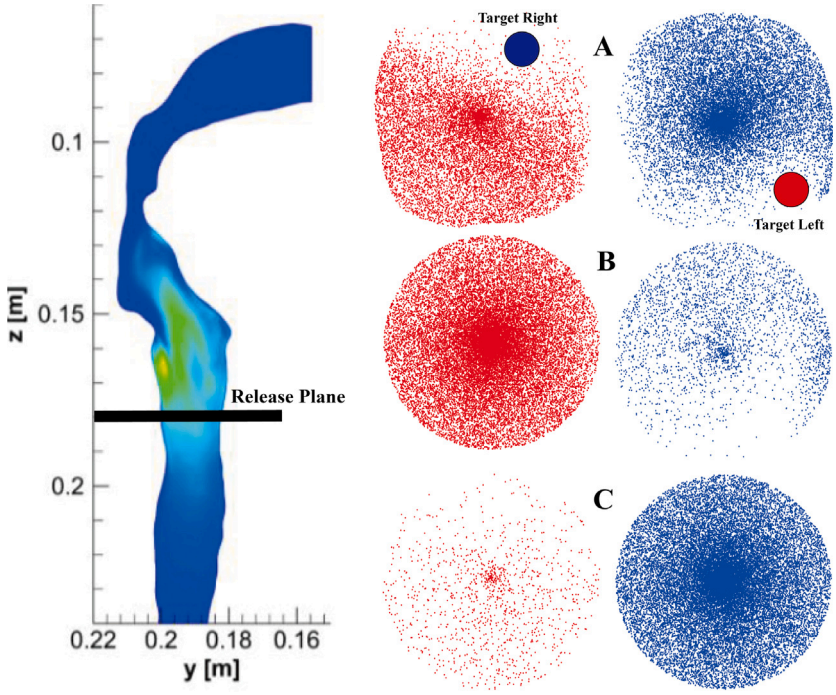

Fig. 14. Reverse tracking of particles (d_p = 10 μm) deposition for the invasive after-larynx approach for the following scenarios: (A) reference case with an uniform particle release, (B) the left lung targeted case, (C) the right lung targeted case. Note the release plane for the after-larynx invasive approach (-left) with contours of the turbulent kinetic energy in central vertical plane.

As a proof-of-concept, a single realistic healthy lung geometry was considered. This approach should be extended to include additional patient-specific geometries that incorporate typical lung pathologies such as asthma, tuberculosis, chronic obstructive pulmonary disease, and others.

In current work, the released spherical particles were assumed to remain unchanged throughout the entire transport process. Potential changes in diameter and shape due to effects temperature and humidity effects, as well as possible particle clusters formation, are recommended for future studies .

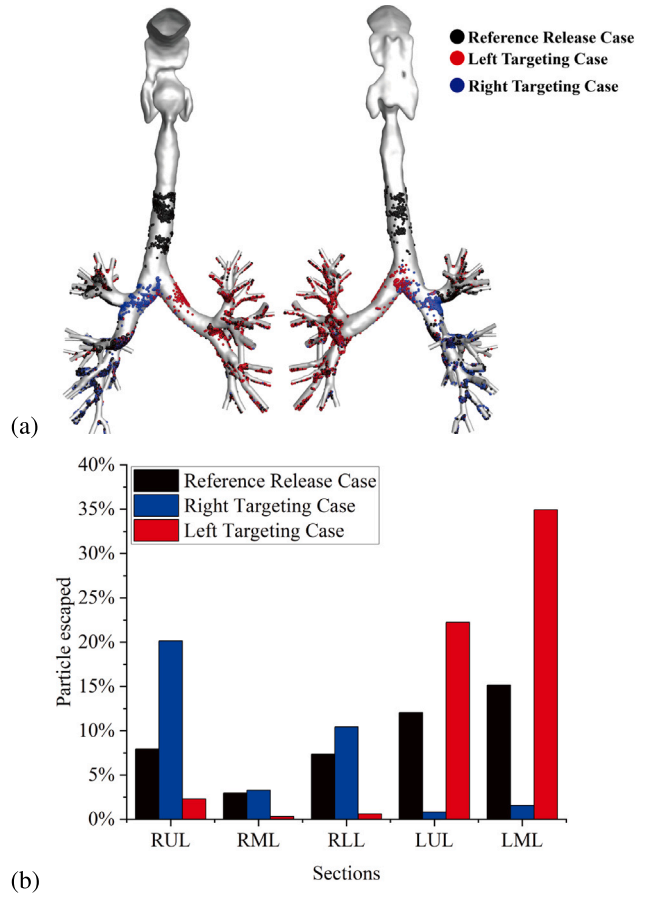

Fig. 15. (a) Visualization of the particles deposition (d_p = 10 μm) for the invasive after-larynx approach for the reference case (black), the left lung targeting (red), the right lung targeting(blue) (a front view — left; a back view — right); Particle deposition visualization for directional targeted release strategy; (b) Sectional escape analysis for directional targeted invasive after-larynx release strategy.

5. Conclusions and outlook

The current study demonstrates the feasibility of applying both invasive and non-invasive release strategies within the upper and central human airways to optimize particle drug delivery performance. The results indicate that concentrating the particle release on specific regions of the inlet mouth plane can improve delivery efficiency by enabling particles to more effectively penetrate the complex flow field in the larynx. Compared to the non-invasive method, the invasive approach achieved a higher level of optimization, resulting in improved deposition performance in monitored airway generations and increased particle escape toward the deeper lung. Directional invasive control was further demonstrated by utilizing specific regions within the release plane (identified through back-tracking of particles, which additionally improved the targeted delivery. Although this research involved certain assumptions and simplifications to accommodate computational resource requirements, it presents a viable approach for patient-specific performance estimation and directional control of particle drug delivery in the lungs. This approach could be valuable in developing novel, breath-powered medical drug delivery systems and treatment workflows for respiratory diseases.

For further investigation, the filtering criteria in the reverse tracking process could consider filtering particles by targeted anatomical sections rather than by directional targeting, as applied in the current research. A more refined division during reverse tracking may help achieve sectional deposition control, enabling drug delivery to specific regions of the lung. This approach will assist in developing more accurate delivery strategies and reduce drug usage during treatment.

List of abbreviations:

CFD -	computational fluid dynamics;
CT -	computed tomography;
DRW -	discrete random walk;
LES -	Large-Eddy Simulation;
LUL -	left upper lobe;
LLL -	left lower lobe;
RANS -	Reynolds-Averaged Navier–Stokes;
RLL -	right lower lobe;
RML -	right middle lobe;
RUL -	right upper lobe;
TD -	turbulent dispersion;

CRediT authorship contribution statement

Ruipeng Xu: Writing – review & editing, Writing – original draft, Visualization, Validation, Software, Methodology, Investigation, Formal analysis, Data curation. **Jiaqi Fan:** Writing – review & editing, Visualization. **Xueren Li:** Writing – review & editing, Methodology. **J. Ruud van Ommen:** Writing – review & editing, Supervision, Conceptualization. **Yidan Shang:** Writing – review & editing, Conceptualization. **Saša Kenjereš:** Writing – review & editing, Writing – original draft, Supervision, Resources, Methodology, Investigation, Conceptualization.

Declaration of competing interest

The authors declare that they have no known competing financial interests or personal relationships that could have appeared to influence the work reported in this paper.

Acknowledgments

The research of Ruipeng Xu was made possible by the financial support of the Chinese Scholarship Council (CSC). We also thank the support of the National Natural Science Foundation of China (Grant No. 82370101).

Data availability

Data will be made available on request.

References

[1] WHO, Ambient (outdoor) air pollution, 2024.
[2] X. Li, Y. Yan, X. Fang, J. Tu, Numerical studies of indoor particulate and gaseous micropollutant transport and its impact on human health in densely-occupied spaces, Environ. Pollut. 342 (2024) 123031.
[3] H. Wu, B. Bai, J. Liu, Temperature-driven coupled transport of pollutants and suspended particles established by granular thermodynamics, Int. J. Heat Mass Transfer (2024).
[4] X. Li, Y. Yan, X. Fang, F. He, J. Tu, Towards understanding of inhalation exposure of pilots in the control cabin environment, Build. Environ. 242 (2023) 110572.
[5] S. Kenjeres, F.S. Henry, A. Tsuda, Is current social distancing enough? Ann. Biomed. Eng. 49 (9) (2021) 1973–1974.
[6] Y. Yan, X. Li, L. Yang, P. Yan, J. Tu, Evaluation of cough-jet effects on the transport characteristics of respiratory-induced contaminants in airline passengers' local environments, Build. Environ. 183 (2020) 107206.
[7] K. Fennelly, Particle sizes of infectious aerosols: implications for infection control, Lancet. Respir. Med. 8 (2020) 914–924.
[8] X. Li, Z. Chen, J. Tu, H. Yu, Y. Tang, C. Qin, Impact of impinging jet ventilation on thermal comfort and aerosol transmission: A numerical investigation in a densely-occupied classroom with solar effect, J. Build. Eng. 94 (2024) 109872.

[9] C. Qi, H. Zhang, Y. Zhu, S. Chen, G. Ran, Study on distributions of airflow velocity and convective heat transfer coefficient characterizing duct ventilation in a construction tunnel, Build. Environ. (2020) 107464.
[10] J. Sanchis, C. Corrigan, M.L. Levy, J.L. Viejo, Inhaler devices–from theory to practice, Respir. Med. 107 (4) (2013) 495–502.
[11] R. Xu, J. de Graaff, S. Kenjeres, Towards optimized drug delivery in simplified and patient-specific lung geometries, in: 10th International Symposium on Turbulence, Heat and Mass Transfer, THMT-23, Rome, Italy, 11-15 September 2023, Begel House Inc., 2023.
[12] J. Capecelatro, W. Longest, C. Boerman, M. Sulaiman, S. Sundaresan, Recent developments in the computational simulation of dry powder inhalers, Adv. Drug Deliv. Rev. 188 (2022) 114461.
[13] M. Rahimi-Gorji, T. Gorji, M. Gorji-Bandpy, Details of regional particle deposition and airflow structures in a realistic model of human tracheobronchial airways: two-phase flow simulation, Comput. Biol. Med. 74 (2016) 1–17.
[14] K. Ahookhosh, M. Saidi, H. Aminfar, M. Mohammadpourfard, H. Hamishehkar, S. Yaqoubi, Dry powder inhaler aerosol deposition in a model of tracheobronchial airways: Validating CFD predictions with in vitro data, Int. J. Pharm. 582 (2020) 119599.
[15] M. Sommerfeld, O. Sgrott, M. Taborda, P. Koullapis, K. Bauer, S. Kassinos, Analysis of flow field and turbulence predictions in a lung model applying RANS and implications for particle deposition, Eur. J. Pharm. Sci. 163 (2021) 105959.
[16] Z. Zhang, C. Kleinstreuer, Airflow structures and nano-particle deposition in a human upper airway model, J. Comput. Phys. 198 (2004) 178–210.
[17] M. Kiasadegh, H. Emdad, G. Ahmadi, O. Abouali, Transient numerical simulation of airflow and fibrous particles in a human upper airway model, J. Aerosol Sci. 140 (2020) 105480.
[18] H. Liu, S., T. Hu, D., Computational investigation of flow characteristics and particle deposition patterns in a realistic human airway model under different breathing conditions, Respir. Physiol. Neurobiol. 314 (2023) 104085.
[19] S. Ghorui, D. Kundu, A. Chakravarty, M. Panchagnula, The impact of asymmetric branching on particle deposition in conducting airways, Int. J. Multiph. Flow 171 (2024) 104935.
[20] H. Jing, X. Cui, A review on numerical studies of airflow dynamics and particle deposition in human respiratory system, Particuology 82 (2024) 72–92.
[21] C. Ou, H. Jian, Q. Deng, Particle deposition in human lung airways: Effects of airflow, particle size, and mechanisms, Aerosol Air Qual. Res. 20 (2020) 167–182.
[22] M. Rahman, M. Zhao, M. Islam, K. Dong, S. Saha, Numerical study of nanoscale and microscale particle transport in realistic lung models with and without stenosis, Int. J. Multiph. Flow 139 (2021) 103842.
[23] Z. Zhang, C. Kleinstreuer, J. Donohue, C. Kim, Comparison of micro- and nano-size particle depositions in a human upper airway model, J. Aerosol Sci. 36 (2005) 211–233.
[24] A. Farghadan, K. Poorbahrami, S. Jalal, J. Oakes, F. Coletti, A. Arzani, Particle transport and deposition correlation with near-wall flow characteristic under inspiratory airflow in lung airways, Comput. Biol. Med. 120 (2020) 103703.
[25] S. Khaksar, M. Paknezhad, M. Saidi, K. Ahookhosh, Numerical modeling of particle deposition in a realistic respiratory airway using CFD-dpm and genetic algorithm, Biomech. Model. Mechanobiol. (2024).
[26] W. Chen, C. Chang, J. Mutuku, S. Lam, W. Lee, Aerosol deposition and airflow dynamics in healthy and asthmatic human airways during inhalation, J. Hazard. Mater. 416 (2021) 125856.
[27] M. Taheri, O. Pourmehran, M. Sarafraz, K. Ahookhosh, A. Farnoud, X. Cui, Effect of swirling flow and particle-release pattern on drug delivery to human tracheobronchial airways, Biomech. Model. Mechanobiol. 20 (2021) 1745–1760.
[28] A. Gurumurthy, C. Kleinstreuer, Helical fluid-particle flow dynamics for controlling micron-particle deposition in a representative human upper lung-airway model, J. Aerosol Sci. 151 (2021) 105656.
[29] A. Negi, S. Nimbkar, J.A. Moses, Engineering inhalable therapeutic particles: Conventional and emerging approaches, Pharmaceutics 15 (2023).
[30] S.K. Shukla, A. Sarode, D.D. Kanabar, A. Muth, N. Kunda, S. Mitragotri, V. Gupta, Bioinspired particle engineering for non-invasive inhaled drug delivery to the lungs., Mater. Sci. Eng. C, Mater. Biological Appl. 128 (2021) 112324.
[31] S. Tanprasert, C. Kampeewichean, S. Shiratori, R. Piemjaiswang, B. Chalermsinsuwan, Non-spherical drug particle deposition in human airway using computational fluid dynamics and discrete element method., Int. J. Pharm. (2023) 122979.
[32] Y. Ostrovski, S. Dorfman, W. Poh, S.C.J. Loo, J. Sznitman, Focused targeting of inhaled magnetic aerosols in reconstructed in vitro airway models., J. Biomech. 118 (2021) 110279.
[33] S. Kenjereš, On recent progress in modelling and simulations of multi-scale transfer of mass, momentum and particles in bio-medical applications, Flow, Turbul. Combust. 96 (3) (2016) 837–860.
[34] S. Kenjereš, J.L. Tjin, Numerical simulations of targeted delivery of magnetic drug aerosols in the human upper and central respiratory system: a validation study, R. Soc. Open Sci. 4 (12) (2017) 170873.
[35] Y. Ostrovski, S. Dorfman, W. Poh, S. Loo, J. Sznitman, Focused targeting of inhaled magnetic aerosols in reconstructed in vitro airway models, J. Biomech. 118 (2021) 110279.
[36] C. Wu, W. Yan, C. Rou, Y. Liu, G. Li, Numerical study on targeted delivery of magnetic drug particles in realistic human lung, Powder Technol. 394 (2021) 887–897.
[37] K. Ahookhosh, M. Saidi, M. Mohammadpourfard, H. Aminfar, H. Hamishehkar, A. Farnoud, O. Schmid, Flow structure and particle deposition analyses for optimization of a pressurized metered dose inhaler (pMDI) in a model of tracheobronchial airway, Eur. J. Pharm. Sci. 164 (2021) 105911.
[38] P. Das, E. Nof, I. Amirav, S.C. Kassinos, J. Sznitman, Targeting inhaled aerosol delivery to upper airways in children: Insight from computational fluid dynamics (CFD), PLoS One 13 (11) (2018) e0207711.
[39] A. Sonnenberg, J. Herrmann, M. Grinstaff, B. Suki, A Markov chain model of particle deposition in the lung, Sci. Rep. 10 (1) (2020) 12947.
[40] N. Khajeh-Hosseini-Dalasm, P. Longest, Deposition of particles in the alveolar airways: Inhalation and breath-hold with pharmaceutical aerosols, J. Aerosol Sci. 79 (2015) 15–30.
[41] P. Koullapis, S. Kassinos, M. Bivolarova, A. Melikov, Particle deposition in a realistic geometry of the human conducting airways: Effects of inlet velocity profile, inhalation flowrate and electrostatic charge, J. Biomech. 49 (11) (2016) 2200–2212.
[42] A. Lancmanová, T. Bodnár, Numerical simulations of human respiratory flows: a review, Discov. Appl. Sci. 7 (4) (2025) 1–74.
[43] S. Neelakantan, Y. Xin, D.P. Gaver, M. Cereda, R. Rizi, B.J. Smith, R. Avazmohammadi, Computational lung modelling in respiratory medicine, J. R. Soc. Interface 19 (191) (2022) 20220062.
[44] H. Jing, H. Ge, L. Wang, Q. Zhou, L. Chen, S. Choi, X. Cui, Large eddy simulation study of the airflow characteristics in a human whole-lung airway model, Phys. Fluids 35 (7) (2023).
[45] E. Nof, S. Bhardwaj, P. Koullapis, R. Bessler, S. Kassinos, J. Sznitman, In vitro–in silico correlation of three-dimensional turbulent flows in an idealized mouth-throat model, PLoS Comput. Biol. 19 (3) (2023) e1010537.
[46] Y. Yan, X. Li, K. Ito, Numerical investigation of indoor particulate contaminant transport using the Eulerian-Eulerian and Eulerian-Lagrangian two-phase flow models, Exp. Comput. Multiph. Flow 2 (2020) 31–40.
[47] M.S. Islam, S.C. Saha, T. Gemci, I.A. Yang, E. Sauret, Z. Ristovski, Y. Gu, Euler-Lagrange prediction of diesel-exhaust polydisperse particle transport and deposition in lung: Anatomy and turbulence effects, Sci. Rep. 9 (1) (2019) 12423.
[48] X. Li, R. Xu, J. Fan, L. Zhang, W. Sun, S. Kenjeres, Y. Shang, W. Yang, Evaluation of multi-output machine learning models for predicting inhaled particle deposition in the human upper and central airway, Powder Technol. 458 (2025) 120924.
[49] A.J. Hickey, H.M. Mansour, M.J. Telko, Z. Xu, H.D. Smyth, T. Mulder, R. McLean, J. Langridge, D. Papadopoulos, Physical characterization of component particles included in dry powder inhalers. I. strategy review and static characteristics, J. Pharm. Sci. 96 (5) (2007) 1282–1301.
[50] P. Rogliani, L. Calzetta, A. Coppola, F. Cavalli, J. Ora, E. Puxeddu, M.G. Matera, M. Cazzola, Optimizing drug delivery in COPD: the role of inhaler devices, Respir. Med. 124 (2017) 6–14.
[51] Y. Guo, H. Bera, C. Shi, L. Zhang, D. Cun, M. Yang, Pharmaceutical strategies to extend pulmonary exposure of inhaled medicines, Acta Pharm. Sin. B 11 (8) (2021) 2565–2584.
[52] C. Kleinstreuer, Z. Zhang, J.F. Donohue, Targeted drug-aerosol delivery in the human respiratory system, Annu. Rev. Biomed. Eng. 10 (2008) 195–220.
[53] M.R. Islam, C. Liu, C. Cai, J. Shah, Y. Feng, A user-centered smart inhaler algorithm for targeted drug delivery in juvenile onset recurrent respiratory papillomatosis treatment integrating computational fluid particle dynamics and machine learning, Phys. Fluids 36 (2) (2024).
[54] M.R. Islam, Y. Feng, Achieving targeted delivery of chemotherapeutic particles to small airway tumors via pulmonary route using endotracheal catheters: A CFPD study, Pharmaceuticals 16 (10) (2023) 1448.
[55] S. Kenjeres, Experimental and computational FHMT for medical diagnostics: towards patient-specific treatment, in: Proceedings of the International Symposium on Turbulence, Heat and Mass Transfer, 2023, p. 15.
[56] A.J. Banko, F. Coletti, D. Schiavazzi, C.J. Elkins, J.K. Eaton, Three-dimensional inspiratory flow in the upper and central human airways, Exp. Fluids 56 (6) (2015) 117.
[57] L. Geronzi, B.M. Fanni, B. De Jong, G. Roest, S. Kenjereš, A parametric 3D model of human airways for particle drug delivery and deposition, Fluids 9 (2) (2024) 47.
[58] R. Monchaux, M. Bourgoin, A. Cartellier, Analyzing preferential concentration and clustering of inertial particles in turbulence, Int. J. Multiph. Flow 40 (2012) 1–18.
[59] ANSYS, ANSYS/Fluent Theory Guide, Ansys Inc., USA 15317 (2011) 724–746.
[60] F.R. Menter, Improved two-equation k-omega turbulence models for aerodynamic flows. NASA STI, Recon Tech. Rep. 93 (1992) 22809.
[61] M.L. Thomas, P.W. Longest, Evaluation of the polyhedral mesh style for predicting aerosol deposition in representative models of the conducting airways, J. Aerosol Sci. 159 (2022) 105851.
[62] V.L. Kolachala, O.A. Henriquez, S. Shams, J.S. Golub, Y.-t. Kim, H. Laroui, E. Torres-Gonzalez, K.L. Brigham, M. Rojas, R.V. Bellamkonda, et al., Slow-release nanoparticle-encapsulated delivery system for laryngeal injection, Laryngoscope 120 (5) (2010) 988–994.